Solid State Phenomena
ISSN: 1662-9779, Vol. 387, pp 53-60
doi:10.4028/p-gBukM0

Submitted: 2026-01-04
Revised: 2026-02-15
Accepted: 2026-02-17
Online: 2026-04-14

Fibre Tension-Induced Stresses in Filament-Wound Composites

Jurui Liu[1,3,a*], Stepan V. Lomov[2,b] , Chung Hae Park[3,c] and Jan Ivens[1,d]

[1]KU Leuven, Department of Materials Engineering Campus De Nayer, J. De Nayerlaan 5, 2860 Sint-Katelijne-Waver, Belgium

[2]KU Leuven, Department of Materials Engineering, Kasteelpark Arenberg 44 box 2450, 3001, Leuven, Belgium

[3]IMT Nord Europe, Institut Mines-Télécom, University of Lille, Centre for Materials and Processes, 59500, Lille, France

Email: [a]jurui.liu@kuleuven.be , [b]stepan.lomov@kuleuven.be, [c]chung-hae.park@imt-nord-europe.fr, [d]jan.ivens@kuleuven.be

Keywords: Filament winding, fibre tension, residual stress

Abstract. Fibre tension is an important process parameter during filament winding. It strongly affects the void content and fibre volume fraction, which in turn determines the mechanical performance of the part. Fibre tension also contributes to the residual stresses that develop in the filament-wound material.

This study focuses on how the fibre tension shapes the stress distribution in filament-wound composites. To this end, a numerical predictive model was developed. Experimental validation was conducted using a force sensor, and good agreement was observed between the model predictions and the experimental measurements. These findings provide deeper insight into the role of fibre tension in filament winding and offer practical guidance for optimising the process to enhance the performance of composite pressure vessels.

Introduction

Filament winding is an advanced composite manufacturing technique that winds continuous fibre tows or prepreg on the mandrel and processes it as high-performance composites. It has been widely used in various industries, including the manufacturing of pressure vessels, aerospace components, as well as sports and recreational equipment.

Several parameters can be independently controlled during the filament winding process, for instance winding speed, fibre tension, and internal pressure in the mandrel. Among these, fibre tension has been identified as a critical factor influencing the quality and performance of filament-wound products [1]. The filament-wound parts manufactured with high fibre tension can have enhanced interlayer compaction, reduced void content, increased fibre volume fraction and consequently improved strength and stiffness of the composite [1–3].

The development of fibre-tension-induced stress during filament winding has been the subject of a number of studies. Early research focused on analytical methods. These analytical models were built upon the plane-stress hypothesis and relied on the superposition principle to represent the incremental build-up of the wound structure [4]. Subsequent developments introduced two-dimensional models based on thick-wall cylinder theory, enabling the estimation of tension-induced stress distributions with accuracy comparable to finite element predictions [5–7]. These models were later extended to a three-dimensional case to better represent the spatially varying stress state in wound composites [8,9].

Apart from analytical modelling, finite element analysis has become a widely adopted tool for predicting fibre-tension-induced stresses. Accurate prediction of tension-induced stress during the winding process requires combining both layer activation and the application of tension within the numerical framework. For this purpose, the birth–death element technique is commonly employed, where newly deposited layers are activated while inactive layers are excluded from the computation [10–12]. Among the available strategies for applying fibre tension, the temperature-parameter method

is particularly prevalent. This approach introduces a virtual coefficient of thermal expansion to the composite layers and applies a negative temperature change to generate a contraction equivalent to the target tension force [7,11,13]. Alternative implementations treat the tension as a predefined stress field combined with the birth–death method, offering more direct load control and improved accuracy in maintaining element thickness during activation [12]. The aforementioned methodologies have advanced the design of tension control and improved the understanding of the influence of fibre tension in filament-wound materials. However, several limitations and challenges remain in the existing studies. Transversely isotropic material properties are commonly adopted for modelling wound materials, including prepregs and fibre tows. The thermal and shrinkage behaviour of these materials is often neglected. The input properties of the wound material, especially those of the fibre tow, have not been fully investigated. Some studies [5,14] obtained the transverse modulus of the fibre tow by fitting numerical results with experimental data. Additionally, limited experimental validation has been reported, and the accuracy of the models has not been thoroughly assessed.

The present model is based on the birth–death element method and the predefined stress method. Track elements were introduced into the numerical model to control layer thickness and improve numerical convergence. Previous work has overlooked the compaction behaviour of fibre tows in determining internal stress development. To address this limitation, a power-law compaction model was incorporated to capture the evolution of the transverse modulus of the fibre tow. Thermal and shrinkage effects are not considered in the current model. We demonstrate the accuracy of the model through comparison with a direct measurement of the radial stress resulting from fibre tension. This study provides a deeper understanding of the fibre tension influence on the filament wound material and a guidance for the optimisation of the filament winding technology.

Experiment

Material and setup

To monitor the stress evolution induced by the fibre tension during the winding process, a thin film force sensor was employed in this study.

The wound material in this study was Toray T700SC-F0E 12K carbon fibre tows, with 0.13 mm thickness and 6.5 mm width. Radial forces acting on the mandrel surface during winding were measured using a Tekscan FlexiForce A201 force sensor with 0.203 mm thickness [15].The experimental setup used to record the radial force is shown in Fig. 1.

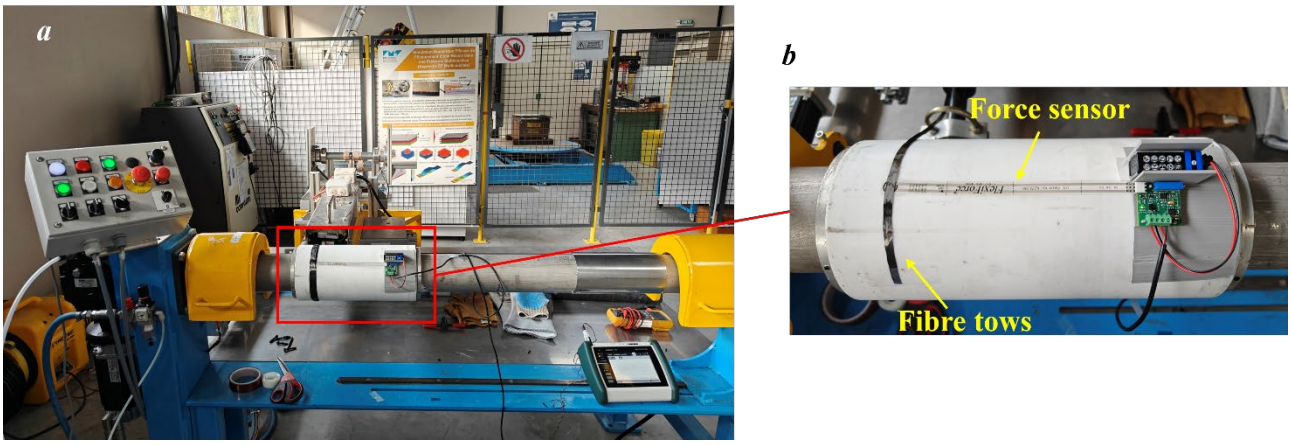

Fig. 1 (a). Overview of the experimental set-up (b). Close-up view showing the force sensor and fibre tows

The mandrel was made of Teflon with a diameter of 150 mm and a thickness of 10 mm. The force sensor was attached to the outer surface of the mandrel at the winding location. A dedicated fixture was designed to accommodate the sensor electronics and wiring, ensuring stable positioning and reliable signal acquisition during the winding process.

Prior to each test, the force sensor was calibrated using known weights. The sensor output voltage varies with the applied normal load on the sensing area, and a calibration curve was established to convert the measured voltage into force values. A constant fibre tension of 10 N was applied during winding, and four repeated tests were conducted to ensure repeatability.
The winding speed was set to 1.6 rpm to minimize dynamic effects. Dry fibre tows were used without resin. Hoop winding was performed over the sensor's sensing area. During the winding process, the fibre tows were continuously wound at the same circumferential position, resulting in a progressive increase in the number of layers. The radial force exerted on the sensor was continuously recorded throughout the winding process.

Model Development

Geometry

The dimensions of mandrel and fibre tow are listed in Table 1. A quarter 2D finite element model representing the winding system was established, as shown in Fig. 2. To accurately capture the stress development in the layers, three elements are meshed through the layer thickness.

Table 1 Dimensions of mandrel and fibre tow

Parameter	Value
Mandrel outer diameter	150 mm
Mandrel inner diameter	130 mm
Fibre tow thickness	0.13 mm
Fibre tow width	6.5 mm

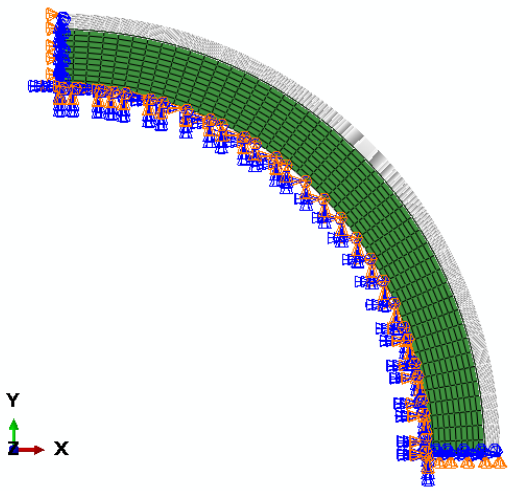

Fig. 2 Finite element model of filament winding system

Boundary Conditions

In the numerical model, the fibre tows were modelled as hoop layers following the experimental hoop-winding configuration. Tie constraints were applied between adjacent fibre tows as well as between the first layer of fibre tows and the mandrel surface, ensuring no slippage occurs during the simulation. This boundary condition is consistent with the no-slippage behaviour typically observed in geodesic winding [16]. Symmetric constraints are imposed on the symmetric surfaces of the model. The inner surface of the mandrel is fixed in accordance with the real situation, where two ends of the mandrel are connected to a central shaft.
A model change was implemented to simulate the material deposition process. Each filament-wound layer was applied in an individual analysis step. In the first analysis step, only the mandrel was

activated. After the initial step, each layer was activated sequentially to mimic the winding process. The equilibrium was continuously updated when a new layer was activated on the mandrel.
During the winding process, the mandrel underwent radial deformation under fibre tension, and the activated layers followed this deformation, whereas the deactivated layers remained fixed. When a new layer was activated, its top surface remained at the undeformed position, while its bottom surface was constrained to the radially displaced surface of the previously activated layer. This mismatch led to artificial stretching of the newly activated layer, resulting in non-physical tensile stresses and unrealistically large thickness strains in the newly activated elements.
To address this issue, a track element method was adopted. All layer elements were duplicated at the same location and shared nodes with the original elements, while their activation sequences were reversed. Initially, all track elements were active, as each wound layer was activated, the corresponding track elements were deactivated and replaced. This procedure enabled the newly activated elements to inherit the deformation history of the previously deposited layers, thereby avoiding artificial stress generation. The overall process is illustrated in Fig. 3.

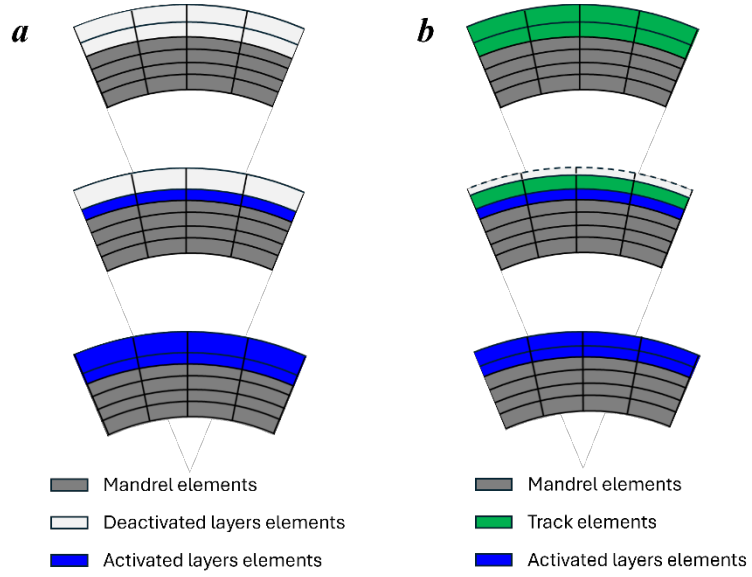

Fig. 3 Illustration for birth-death element method and track elements approach. (a) Traditional birth-death element method. (b) Birth-death element method with track elements

The method was implemented by modifying the input file using the elcopy keyword. To minimise their influence, the track elements were assigned isotropic material properties with a low stiffness of 100 MPa, which was chosen based on the parameter sensitivity analysis.
The fibre tension was applied via a predefined stress field. The fibre tension induced stress in the fibre direction can be obtained through the following equation:

$$\sigma = \frac{T}{t \cdot w} \tag{1}$$

where σ is the fibre tension stress in the layers, T is the applied tension force, t and w are the thickness and width of the fibre tow, respectively.

Material Properties

The mandrel was made of Teflon, whose properties are listed in Table 2.

Table 2 Material properties of mandrel

Parameter	Symbol	value
Young's modulus	E	500 MPa
Poisson's ratio	v	0.45

The material properties of Toray T700 fibre were taken from the datasheet [17]. The in-plane shear modulus was taken from the literature [18]. Hahn [5] and Kempner [19] obtained the transverse modulus by fitting the numerical results to experimental data. They reported that the transverse modulus is fibre-tension-dependent, and the magnitude is much smaller than the longitudinal modulus. To accurately determine the transverse modulus, the compaction behaviour of fibre tow was considered in this model. In filament winding, compaction arises from radial pressure acting on the bottom surface due to force equilibrium, as well as from pressure applied at the top surface when a new layer is wound. The power law for pressure-fibre volume fraction dependency, commonly used in literature (e.g. [20,21]) captures the evolution of fibre volume fraction under different levels of compaction, except at the initial stage where no compaction is applied. In the absence of compaction, this formulation leads to a small non-physical transverse stress. Therefore, a tangent modulus formulation was adopted in the simulation to update the stress: the transverse modulus during the compaction process can be expressed as:

$$E_T = \frac{d\sigma_{33}}{d\varepsilon_{33}} = ab\left(\frac{V_{f0}}{\exp(\varepsilon_{33})}\right)^b \quad (2)$$

where E_T is transverse modulus, σ_{33} is the transverse stress, and $\sigma_{33} = -P$ (P being the compaction pressure) , ε_{33} is transverse strain, V_{f0} is initial fibre volume fraction.

The transverse modulus of fibre tow was evaluated during the simulation by incorporating equation (2) into ABAQUS via UMAT user subroutine. The input parameters a and b were obtained from the literature [20], where they were identified from compaction experiments on dry carbon fibre tows. The input data for the fibre tows are summarized in Table 3.

Table 3 Input material data for T700 fibre tow

Parameter	Symbol	value	Unit
Fibre longitudinal modulus	E_f	230 000	MPa
Poisson's ratio	v_{12}	0	
In-plane shear modulus	G_{12}	4980	MPa
Initial Fibre volume fraction	V_{f0}	0.40	
Power law parameter	a	4975	MPa
Power law parameter	b	13.42	

Results and Discussion

The experimental and simulation results of radial pressure on the outer surface of the mandrel are presented in Fig. 4.

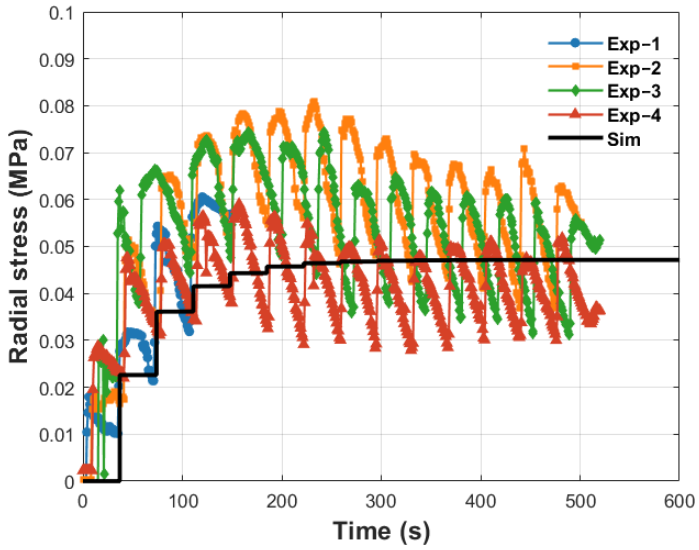

Fig. 4 Numerical and experimental results

The results show that the model can accurately capture both the initial stress development and final saturation behaviour. The corresponding numerical hoop and radial stress distribution through the thickness of the composite layers are presented in Fig. 5. The hoop stress remains tensile throughout the thickness. The stress decreases from the innermost layer to nearly zero between the 6^{th} and 11^{th} layers, and then increases to approximately 10 MPa toward the outer layer. The radial stress decreases from the innermost layer and remains at approximately 0.02 MPa from the 2^{nd} layer to the 18^{th} layer, before dropping to zero at the outer surface. These results indicate that the compaction capability of fibre tow is limited, and that the increasing number of winding layers cannot further increase the radial stress in the previously wound layers.

In addition to stress prediction, the model also provides the fibre volume fraction distribution along the thickness direction, as well as the thickness of each wound layer after completion of the winding process. The predicted fibre volume fraction distribution is shown in Fig. 6. The results show that the fibre volume fraction distribution follows the radial stress pattern: higher compaction forces in the inner layers lead to higher fibre volume fractions, while lower compaction levels are observed towards the outer layers. The predicted thickness of the wound layers and the fibre volume fraction distribution will be validated in future experimental work.

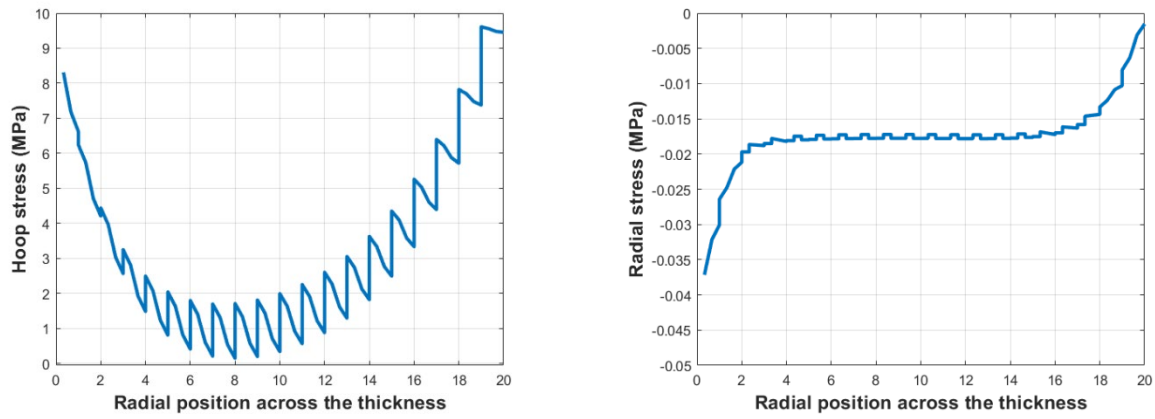

(a) (b)

Fig. 5 Fibre tension induced stress distribution across thickness (a) Hoop stress and (b) Radial stress. The radial coordinate is discretised by the layer index after winding completion, where 0 corresponds to the inner surface of the wound material.

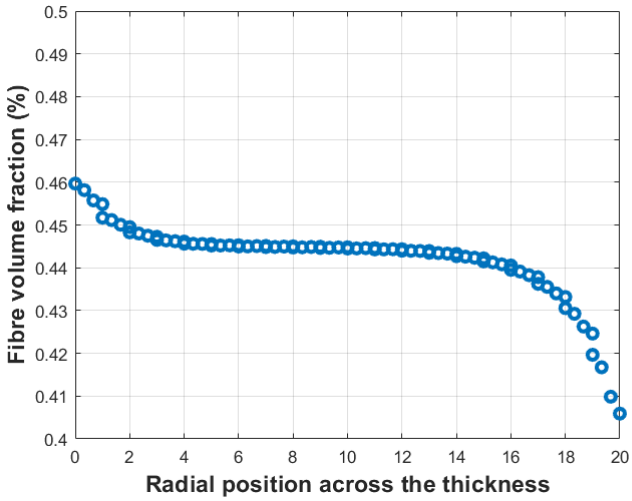

Fig. 6 Predicted fibre volume fraction distribution across thickness after winding completion

Conclusion

In this study, a numerical model was presented to predict the fibre tension induced stress. Birth-death element and predefined stress were used to simulate the winding process and application of fibre tension. Track elements were implemented to accurately capture the thickness of wound layers and stress development. The consolidation behaviour of the fibre tow during the winding process was considered into the model by a power law. A validation experiment using a force sensor on the mandrel surface was performed to record the radial stress development on the outer surface of the mandrel during the winding process. The good agreement between the predicted and experimental results demonstrates the reliability of the model. The validated model thus provides a useful tool for optimizing process parameters and improving product quality in filament winding.

Acknowledgements

This work has been performed within the framework of the ECOHYDRO project (Grant No. 101138008), which is financially supported by the Clean Hydrogen JU and the European Commission through the Horizon Europe program.

References

[1] Cohen D. Influence of filament winding parameters on composite vessel quality and strength. Composites Part A: Applied Science and Manufacturing 1997; 28: 1035–47. https://doi.org/10.1016/S1359-835X(97)00073-0.

[2] Mertiny P, Ellyin F. Influence of the filament winding tension on physical and mechanical properties of reinforced composites. Composites Part A: Applied Science and Manufacturing 2002; 33: 1615–22. https://doi.org/10.1016/S1359-835X(02)00209-9.

[3] Błachut A, Kaleta J, Detyna J, Kmiecik B, Ziętek G, Panek M, et al. Multiscale analysis of composite pressure vessel structures wound with different fiber tensile force. Composite Structures 2024; 337:118065. https://doi.org/10.1016/j.compstruct.2024.118065.

[4] Lee S-Y, Springer GS. Filament Winding Cylinders: I. Process Model. Journal of Composite Materials 1990;24:1270–98. https://doi.org/10.1177/002199839002401202.

[5] Hahn HT, Kempner EA, Lee SS. The stress development during filament winding of thick cylinders. Composites Manufacturing 1993;4:147–56. https://doi.org/10.1016/0956-7143(93)90099-t.

[6] Kang C, Shi Y, Deng B, Yu T, Sun P. Determination of Residual Stress and Design of Process Parameters for Composite Cylinder in Filament Winding. Advances in Materials Science and Engineering 2018;2018:1821342. https://doi.org/10.1155/2018/1821342.

[7] Zu L, Xu H, Zhang B, Li D, Wang H, Zi B. Filament-wound composite sleeves of permanent magnet motor rotors with ultra-high fiber tension. Composite Structures 2018;204:525–35. https://doi.org/10.1016/j.compstruct.2018.07.119.

[8] Liu C, Shi Y. Analytical model for the winding process-induced residual stresses of the multilayered filament wound cylindrical composite parts. Mater Res Express 2019;6:105354. https://doi.org/10.1088/2053-1591/ab3ef8.

[9] Liu C, Shi Y. Design optimization for filament wound cylindrical composite internal pressure vessels considering process-induced residual stresses. Composite Structures 2020;235:111755. https://doi.org/10.1016/j.compstruct.2019.111755.

[10] Zu L, Xu H, Zhang B, Li D, Zi B. Design of filament-wound composite structures with arch-shaped cross sections considering fiber tension simulation. Composite Structures 2018;194:119–25. https://doi.org/10.1016/j.compstruct.2018.04.018.

[11] Zu L, Xu H, Zhang Q, Jia X, Jin S, Li D. Investigation on mechanical behavior of composite electromagnetic gun barrel based on the high tension winding. Composite Structures 2020;248:112521. https://doi.org/10.1016/j.compstruct.2020.112521.

[12] Xie X, Xie X, Li H, Shen L, Zhu J, Yu H, et al. Tension relaxation during the NOL ring winding process based on a novel tracking element method. Journal of Reinforced Plastics and Composites 2024:07316844241278554. https://doi.org/10.1177/07316844241278554.

[13] Xu H, Wang Y, Song H, Li K, Hu J. Analysis of fiber stresses during high-tension winding molding of thermoplastic composites. Journal of Thermoplastic Composite Materials 2025:08927057251318714. https://doi.org/10.1177/08927057251318714.

[14] Kempner EA, Hahn HT. The Effect of Radial Stress Relaxation on Fiber Stresses in Thick Filament-Wound Cylinders n.d.

[15] Tekscan Inc. FlexiForce A201 Sensor Datasheet. (Rev I). Available at: https://www.tekscan.com/sites/default/files/resources/FLX-Datasheet-A201-RevI_1.pdf (accessed 11 December 2025).

[16] Wang R, Jiao W, Liu W, Yang F, He X. Slippage coefficient measurement for non-geodesic filament-winding process. Composites Part A: Applied Science and Manufacturing 2011;42:303–9. https://doi.org/10.1016/j.compositesa.2010.12.002.

[17] Toray Composite Materials America, Inc., T700G Technical Data Sheet, Technical datasheet, 2021. Available at: https://www.toraycma.com/wp-content/uploads/T700G-Technical-Data-Sheet1.pdf

[18] Ng S-P, Tse P-C, Lau K-J. Numerical and experimental determination of in-plane elastic properties of 2/2 twill weave fabric composites. Composites Part B: Engineering 1998;29:735–44. https://doi.org/10.1016/S1359-8368(98)00025-0.

[19] Kempner EA, Hahn HT. Effect of radial stress relaxation on fibre stress in filament winding of thick composites. Composites Manufacturing 1995;6:67–77. https://doi.org/10.1016/0956-7143(95)99646-A.

[20] Lu S, Evans A, Turner T. Analysis of roller compaction pressure distribution in automated dry fibre placement. Composite Structures 2023; 316: 117048. https://doi.org/10.1016/j.compstruct.2023.117048.

[21] Robitaille F, Gauvin R. Compaction of textile reinforcements for composites manufacturing. I: Review of experimental results. Polymer Composites 1998; 19: 198-216. https://doi.org/10.1002/pc.10091.

The publication of this article was funded by the KU Leuven 10.13039/501100004040